

$$\frac{U^2}{2} + \Pi(p) = Const \quad (15)$$

Where, U is the velocity at an arbitrary point of the flow (stream), $\Pi(p)$ is the potential energy of a unit mass at this point:

$$\Pi(p) = \int_p^{p_\infty} \frac{dp}{\rho(p)} \quad (16)$$

Apply the Bernoulli equation to the flow along a streamline from point (p, ρ, V) at vent cross section to point $(p_\infty, \rho_\infty, V_\infty=0)$ of the undisturbed exterior air yields:

$$\frac{V^2}{2} + \int_p^{p_\infty} \frac{dp}{\rho(p)} = 0 \quad (17)$$

In view of the Poisson adiabat (Equations (12) and (17)) leads to the following equation:

$$V = \sqrt{2 \frac{\gamma}{\gamma-1} \frac{p_\infty}{\rho_\infty} \left[\left(\frac{p}{p_\infty} \right)^\frac{\gamma-1}{\gamma} - 1 \right]} \quad (18)$$

The integration of Equation (13) with the initial condition (Equation (14)) in view of Equation (18) yields the mass time history, $M(t)$. The corresponding pressure time history is calculated according to Equation (19) as:

$$P(t) = P_\infty \left(\frac{M(t)/\Theta}{\rho_\infty} \right)^\gamma \quad (19)$$

Figure 11 shows the comparison of the simulation and measured pressure results two sample cases (2.0kg, RP5 gauge, 4.0kg, RP3 gauge). It can be seen that the developed simplified approach based on the Bernoulli equation is well suited for simulation of quasi stationary phase of partially confined explosions (corresponding to a late time) and properly describes the pressure relief and gas outflow from the vented room.

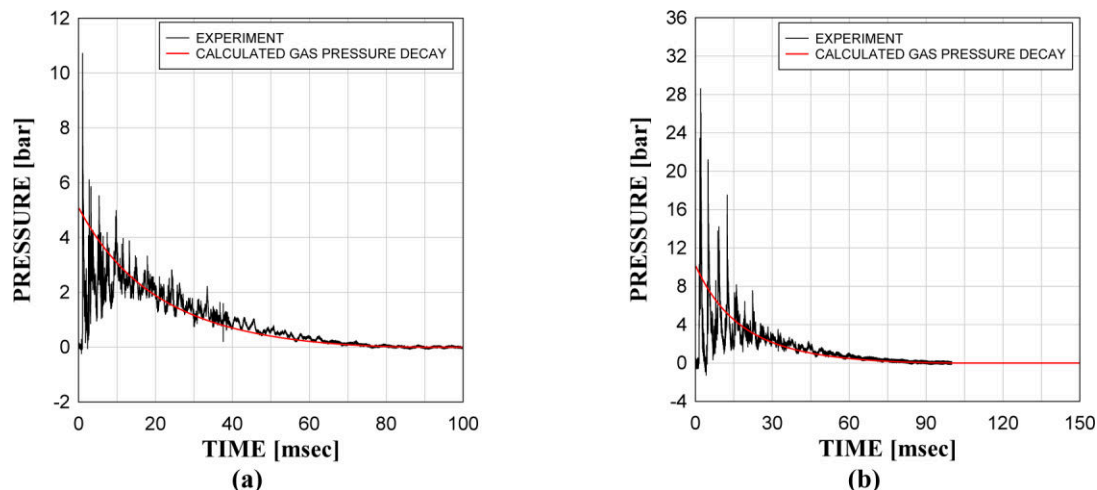


Figure 11. Comparison for the pressure decay between the test result and the calculation result using Bernoulli method (a) 2.0kg, RP5 gauge (b) 4.0kg, RP3 gauge

SUMMARY AND CONCLUSIONS

- Experimental analyses of TNT explosions in a rectangular room with rigid walls and limited venting have been carried out. A series of five blast tests were performed in an instrumented test structure. This study yielded high quality pressure signals at different locations that was used as a data base for comparisons with the computational results.
- Understanding of the afterburning energy release process, as a result of exothermic reaction of some of the detonation products with the oxygen in the air, at certain temperature conditions, helped to improve the numerical simulations when this afterburning energy was included into the equation of state of the explosive during an appropriate time interval.
- The theoretical work includes thermo-chemical analysis of the energetic properties of the explosive in an attempt to evaluate the afterburning energy release and its dependence on different conditions. It also includes an analytical derivation of the residual gas pressure magnitude that is based on the ideal gas equation of state. This model predicts the gas pressure as function of the exploded charge weight per unit volume of the confined space. The model takes into account the number of moles produced in the detonation process and uses the laws of thermodynamics to find the blast temperature. This is a new theoretical approach that explains experimental results and agrees well with empirical findings.
- A method for calculating the gas pressure decay, based on Bernoulli theory, was developed for a partially confined explosion. The derived formulas are found to yield gas pressure predictions that agree well with our experimental results and with experimental results available in the open literature.
- This study contributes to understanding the relationship between explosion data and its results, and has a great value in advancing knowledge on this subject. Beyond that, it contributes to more accurately design of buildings subjected to such conditions discussed, which today are designed with simplified and approximate design tools which their suitability is questionable.

REFERENCES

- A718300 (1974): Engineering Design Handbook. Explosions in Air. Part One. Army Materiel Command Alexandria, VA
- AASTP-1 (2006): Manual of NATO Safety Principles for the Storage of Military Ammunition and Explosives, NATO International Staff – Defense Investment Division.
- Baker W.E., Cox P.A., Westine P.S., Kulesz J.J., Strehlow R.A. (1983), Explosion hazards and evaluation, Elsevier, Amsterdam.
- Bangash M.Y.H. (1993) Impact and Explosion. Analysis and Design. Spon Press: Blackwell Scientific Publications, Oxford.
- Ben-Dor G., Igra O., Elperin T. (2000), Handbook of Shock Waves. Academic Press: Elsevier.
- Bryan J., Steward B.S. (2006). Reproducibility, Distinguishability, and Correlation of Fireball and Shockwave Dynamics in Explosive Munitions Detonations, Master Thesis.
- Chock J.M.K., Kapania R.K. (2001). Review of two methods for calculating explosive Air blast. The Shock and vibration digest. Vol. 33(2), pp. 91–102.
- Cooper P.W. (1996). Explosives Engineering, Wiley-VCH, Toronto.
- Corneliu B. (2004). Evaluation and rehabilitation of a building affected by a gas explosion.

- Progress in Structural Engineering and Materials. Vol. 6(3), pp. 137–146
- Dewey J.M. (1964). The air velocity in blast waves from TNT explosions. Proceedings of the Royal Society of London, A, 279:(1378) 366–385.
- Dorn M., Nash M., Anderson G., Jones N., Brebbia C.A. (1996). The Numerical Prediction of the Collapse of a Complex Brick Building Due to an Internal Explosion, ASME Publications-PVP, Vol. 351, pp. 359–364.
- Edri I., Savir Z., Feldgun V.R., Karinski Y.S., Yankelevsky D.Z. (2011). On Blast Pressure Analysis Due to a Partially Confined Explosion: I. Experimental Studies. International Journal of Protective Structures, Vol. 2(1), pp. 1–20.
- Edri I., Feldgun V.R., Karinski Y.S., Yankelevsky D.Z. (2012). On Blast Pressure Analysis Due to a Partially Confined Explosion: III. Afterburning Effect. International Journal of Protective Structures, Vol. 3(3), pp.311-332.
- Edri I., Feldgun V.R., Karinski Y.S., Yankelevsky D.Z. (2013). Afterburning Aspects in an Internal TNT Explosion. International Journal of Protective Structures. Vol. 4(1), pp.96-116.
- Feldgun V.R., Karinski Y.S., Yankelevsky D.Z. (2011a). Some Characteristics of an Interior Explosion within a Room without Venting. Structural Engineering and Mechanics, An International Journal, Vol. 38 (5), pp.633–649.
- Feldgun V.R., Karinski Y.S., Yankelevsky D.Z. (2011b). A simplified model with lumped parameters for explosion venting simulation. International Journal of Impact Engineering, Vol. 38, pp.964–975.
- Feldgun V.R., Karinski Y.S., Edri I., Yankelevsky D.Z. (2012). On Blast Pressure Analysis Due to a Partially Confined Explosion: II. Numerical Studies. International Journal of Protective Structures, Vol. 3(1), pp. 61–79.
- Griffiths H., Pugsley A., Saunders O. (1968) Report of the Inquiry into the “Collapse of Flats at Ronan Point, Canning Town”, HMSO.
- Kinney G.F. (1962). Explosive shocks in air. The Macmillan Co., New York.
- Luccioni B.M., Ambrosini R.D., Danesi R.F. (2006). Failure of a reinforced concrete building under blast loads. WIT Transactions on Engineering Sciences, Vol.49, pp. 336–345.
- Swisdak M. Jr. (1975). Explosion Effects and Properties. Part I. Explosion Effects in Air. Final Report, A445810.
- O’Daniel J.L., Krauthammer T. (1997). Assessment of numerical simulation capabilities for medium–structure interaction systems under explosive loads. Computers and Structures. 63(5), pp. 875 87.
- Savir Z., Edri I., Feldgun V.R., Karinski Y.S., Yankelevsky D.Z. (2009). Blast Pressure Distribution on Interior Walls Due to a Partially Confined Explosion, International Workshop on Structure Response to Impact and Blast (IWSRIB), Haifa, Israel, November 15-17, 2009.
- UFC-3-340-02 (2008), Structures to Resist the Effects of Accidental Explosions, Department of Defense, December 2008.
- TM-5-1300 (1990): Structures to Resist the Effects of Accidental Explosions. Dept. of the Army, the NAVY and the Air Force, Washington, DC, USA.
- TM-5-855-1 (1986). Fundamentals of Protective Design for Conventional Weapons. Department of Army, Washington, DC, USA.
- UFC 3-340-02 (Unified Facilities Criteria) (2008): Structures to Resist the Effects of Accidental Explosions. Dept. of the Army, the NAVY and the Air Force, Washington, DC, USA.
- Vaidogas E. R. (2003). Pressure Vessel Explosions inside Buildings: Assessing Damage Using Stochastic Accident Simulation. Structural Engineering International, Vol.13 (4), pp. 249–

253.

Weibull H.R.W (1968), Pressures Recorded in Partially Closed Chambers at Explosion of TNT Charges (U). Annals of the New York Academy of Sciences, Vol. 152, Art. 1, pg. 357, 1968.

Impact Behaviour of Sandwich Panels Made of Flax Fiber-Reinforced Bio-Based Polymer Face Sheets and Foam Cores

Dillon J. Betts¹; Pedram Sadeghian, M.ASCE²; and Amir Fam, F.ASCE³

¹Ph.D. Student, Dept. of Civil and Resource Engineering, Dalhousie Univ., 1360 Barrington St., Halifax, NS B3H 4R2, Canada. E-mail: dillonbetts@dal.ca

²Assistant Professor and Canada Research Chair in Sustainable Infrastructure, Dept. of Civil and Resource Engineering, Dalhousie Univ., 1360 Barrington St., Halifax, NS B3H 4R2, Canada (corresponding author). E-mail: pedram.sadeghian@dal.ca

³Donald and Sarah Munro Chair Professor in Engineering and Applied Science and Associate Dean (Research and Graduate Studies), Dept. of Civil Engineering, Queen's Univ., Kingston, ON K7L 3N6, Canada. E-mail: amir.fam@queensu.ca

ABSTRACT

In this paper, the impact behaviour of sandwich panels constructed of flax fibre-reinforced polymer (FFRP) facings and closed cell polyisocyanurate foam cores is studied. A total of 27 sandwich beam specimens (1200 mm long and 150 mm wide) made of 75 mm thick foam have been fabricated. As a part of this study, three of these specimens have been tested under impact load at several energy levels. The main test parameter is the facing thickness (one, two, or three layers of FFRP). A bidirectional flax fabric (400 g/m²) was used for the face sheets and a foam with a density of 64 kg/m³ was used for the core. A bio-based epoxy resin, with an approximate bio-content of 30%, was used to make the FRP facings. Each specimen was tested multiple times increasing the kinetic energy until failure. The kinetic energy was increased by first increasing the drop height and then, if necessary, adding additional weight to the impactor and resetting the height to keep the increase in energy constant. The acceleration of the impactor, the drop weight velocity, and the top and bottom facing strains at mid-span will be measured. It is expected that ultimate energy absorption and strength of the specimens will increase as both the core density and facing thickness increase. The aim of this paper is to provide data to the field of study, provide insight into the structural behavior of these types of structures, and show their viability for use in infrastructure. With further research, there is the potential that these types of structures could be included in structural building codes. This research is part of a larger on-going study and more results will be available at the time of the conference.

INTRODUCTION

To accommodate the increasing interest in sustainability, new infrastructure should incorporate environmentally friendly materials. Using natural materials to make sandwich panels for building cladding and roof slabs is one way to do this. An example of using natural materials in structures is the use of flax fibers to make fiber-reinforced polymers (FRPs) for use as face sheets for structural sandwich panels. Flax fibers are commercially available, are relatively strong and stiff when compared with other plant fibers and have a lower embodied energy than traditional fibers, such as glass and carbon (Cicala et al. 2010). Sandwich panels with flax FRP (FFRP) faces have been studied recently under flexural loading (Betts et al. 2017; Fam et al. 2016; Mak et al. 2015; Sadeghian et al. 2016) and under axial loading (Codyre et al. 2016).

One potential application of these sandwich structures is building cladding systems which can be subjected to impacts from flying debris during a storm event. There have been studies on

the impact behavior of sandwich structures with synthetic FRP faces (Atas and Potoglu 2016; Schubel et al. 2005; Torre and Kenny 2000), but there are no studies into the behavior of sandwich structures with FFRP faces under impact. Therefore, the aim of the current study is to provide an understanding of the behavior of sandwich structures with FFRP faces under impact loading.

EXPERIMENTAL PROGRAM

Test Matrix

As a part of this study, three test specimens were tested under impact with a 10.413 kg drop weight until ultimate failure. Each specimen was tested multiple times, increasing the energy of each subsequent impact. The energy was increased by increasing the initial height of the drop weight. The test parameter was the effect of facing thickness on energy absorption and mechanical properties under impact loading. The test matrix is shown in Table 1.

Table 1. Test Matrix

No.	Specimen I.D.	Number of Layers	Core Density (kg/m ³)
1	1FL-P400	1	64
2	2FL-P400	2	64
3	3FL-P400	3	64

Note: FL = Flax Layers, P400 = 64 kg/m³ core density

The first specimen tested was 2FL-P400. In this test the drop height started at 300 mm and was increased in increments of 300 mm until failure. Upon examination of the data, it was determined that in order to capture the damage initiation and to get a more accurate ultimate energy level, a smaller drop height increment was required. Therefore, specimens 1FL-P400 and 3FL-P400 were tested with drop height increments of 100 mm.

Specimen Fabrication

The specimens were fabricated as a part of a larger study and the specimen fabrication process is discussed extensively in the former studies by (Betts et al. 2017). The closed-cell polyisocyanurate foam cores were supplied in 1200 mm by 2400 mm boards (manufacturer: Elliott Company, Indianapolis, IN, USA). To make the specimens, the foam boards were cut down to a size of 600 mm by 1200 mm and the top and bottom surfaces were cleaned and prepared for fabrication. A layer of the bio-based epoxy (manufacturer: Entropy Resins, Hayward, CA, USA) was then applied followed by a layer of bidirectional flax fabric with a nominal areal mass of 400 g/m² (manufacturer: Composites Evolution, Chesterfield, UK). Additional epoxy was applied to the flax fabric until saturation and additional layers of flax fabric were placed as required. In order to provide a flat finish, a layer of parchment paper was applied to the surface and extra resin and air was removed with a roller. The specimens were allowed to cure for seven days at which point the process was repeated for the opposite surface. After both faces had cured, the specimens were cut down to their final size of 1200 mm long by 150 mm wide using a band saw. The fabrication process is presented in Figure 1.

Test Set-up

To complete the testing, a test set-up was designed and built. This test set-up is shown in Figure 1. As shown in Figure 1, the specimen deflections were measured with a string-type displacement gauge and the top and bottom facing strains were measured with strain gauges located at midspan. A high-speed camera with a frame rate of 500 fps was used to record each impact.



Figure 1. Specimen Fabrication (a) Cleaned Foam and Epoxy (d) Epoxy Preparation (c) Application of Epoxy (d) Application of Flax Fabric (e) Application of Parchment Paper (f) Application of Strain Gauges – Courtesy of Dillon Betts and Pedram Sadeghian

RESULTS AND DISCUSSIONS

The specimen stiffness, damping coefficient, maximum deflection, and maximum facing strains are presented against the impact energy in Figure 3. The impact energy absorption of the panels increased with facing thickness. Before failure, 1FL-P400 resisted a maximum impact of

30.6 Joules (J), 2FL-P400 resisted a maximum impact of 122.6 J, and 3FL-P400 resisted a maximum impact of 172.7 J.

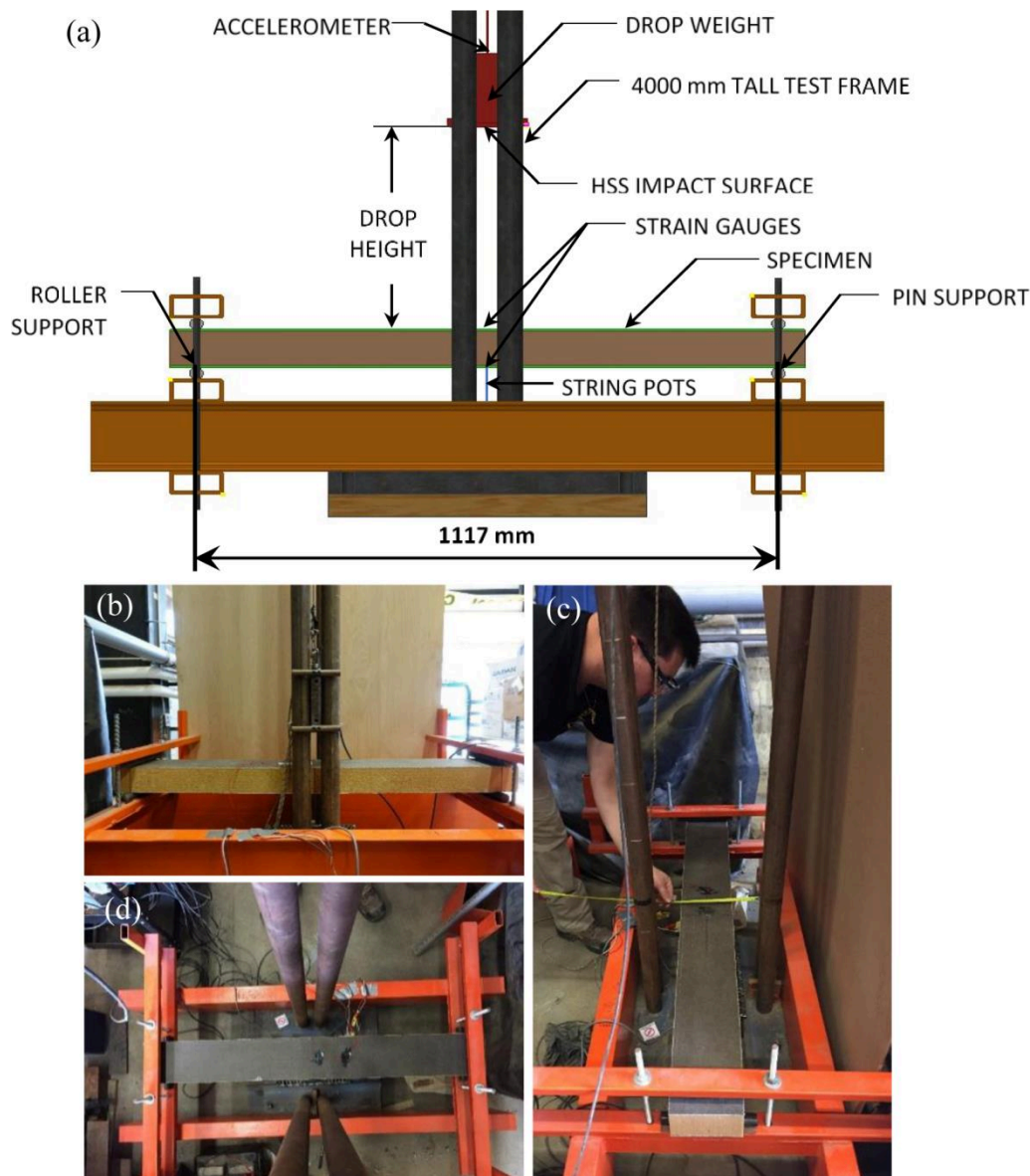


Figure 2. Test Set-up (a) Model (b) Side View (c) End View (d) Top View – Courtesy of Dillon Betts and Pedram Sadeghian

Figure 3a shows the effect of impact energy on the specimen stiffness which was calculated using the following equation:

$$K = \frac{\omega^2 mL}{2}$$

where K is the specimen stiffness, ω_n , is the angular frequency, m is the mass of the specimen in kg/m and L is the span length. Before failure, the specimens' stiffness remained relatively constant and as expected, the stiffness increased with facing thickness. At an impact energy of 40.9 J, the compression face of specimen 1FL-P400 failed beside the drop weight and the stiffness was reduced by approximately 27%. The specimen was tested after failure at impact

energies of 51.1 J and 61.3 J. As the specimen was already damaged, the stiffness was reduced by approximately 76% at these post-failure tests.

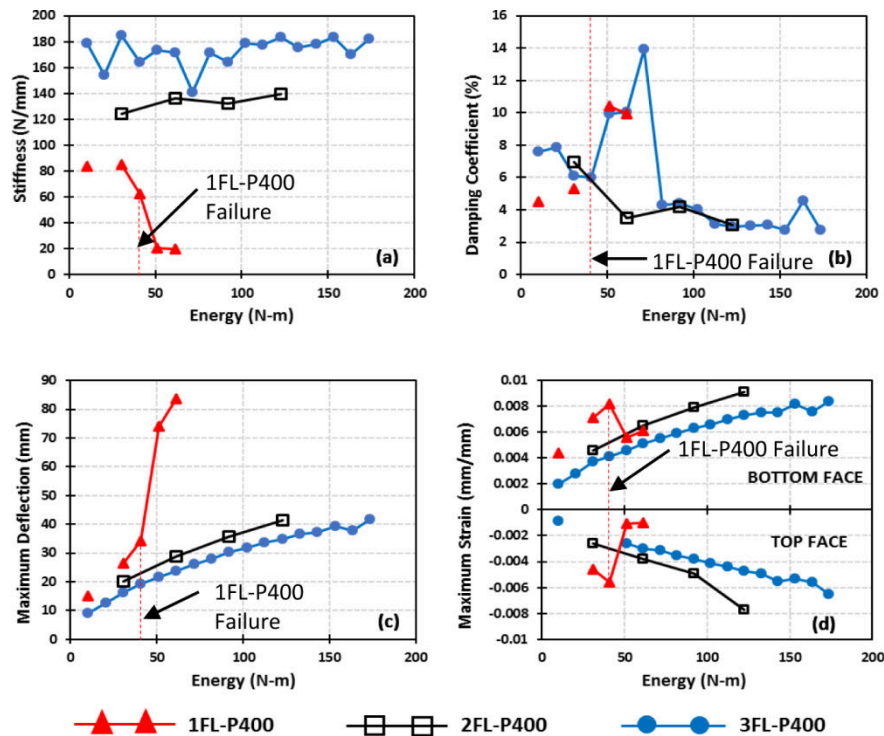


Figure 3. Test Results at Each Energy Level (a) Stiffness (b) Damping Coefficient (c) Maximum Deflection (d) Maximum Facing Strains

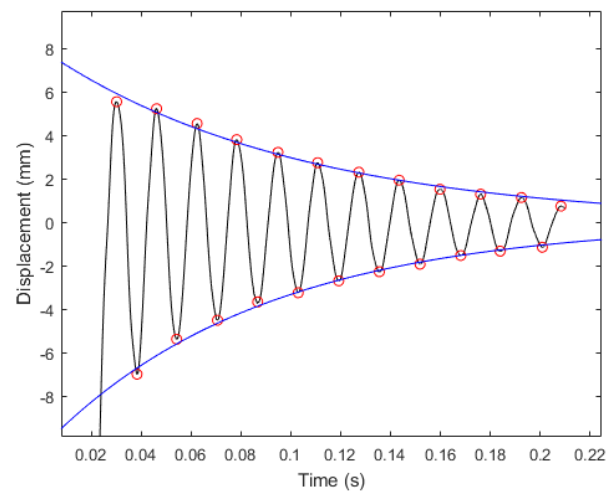


Figure 4. Calculation of Damping Coefficient

Figure 3b shows the damping coefficient versus the impact energy. The damping coefficient was calculated by fitting an exponential curve to the peaks of the deflection data during the free vibration after the first impact as shown in Figure 4. The equation for this curve is:

$$f(t) = Ce^{-\xi\omega_n t}$$

where C is a constant, ξ is the damping coefficient, ω_n is the natural angular frequency of the specimen and t is time. After fitting the curve, the value of the exponential coefficient was

determined and ξ could be calculated. Specimens 2FL-P400 and 3FL-P400 show that as the impact energy increases there is a downward trend in the damping coefficient. Specimen 1FL-P400 shows that after the failure of the top face, there was an increase in damping coefficient.

Figure 3c shows a plot of the measured maximum deflection versus the impact energy. For each specimen, the deflection increased with impact energy. After initial failure, the deflection of specimen 1FL-P400 increased drastically.

As shown in Figure 3d, the facing strains of specimens 2FL-P400 and 3FL-P400 increase as the impact energy increases. After initial failure, the facing strains in specimen 1FL-P400 decreased in the next impact and then began to increase again in subsequent impacts.

Failure Modes

Identical specimens have been tested under static loading by Betts et al. (2017a). Figure 5 shows a comparison of the dynamic failure modes compared to the failure modes of the static tests. Specimens 1FL-P400 and 3FL-P400 show similar failure patterns as their static counterparts, but specimen 2FL-P400 exhibits a different failure mode: tensile rupture and core shear. The static test specimen failed by compression face wrinkling.

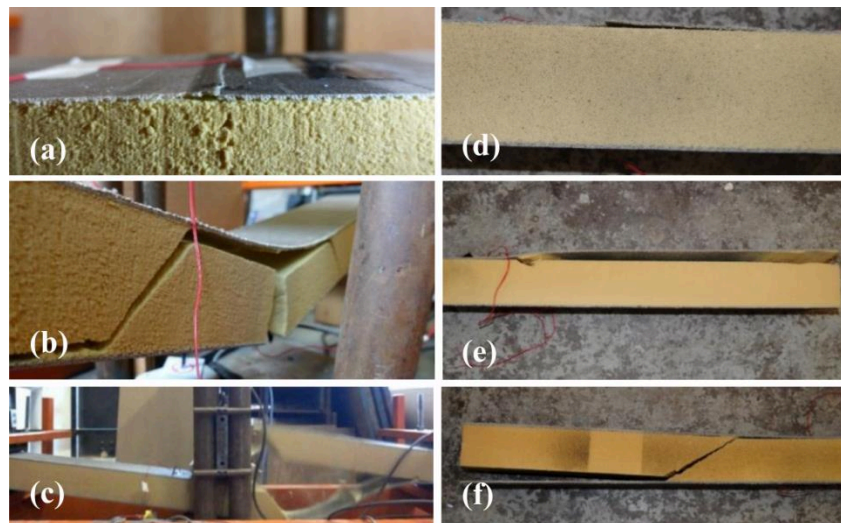


Figure 5. Failure Modes (a Dynamic 1FL-P400 (b) Dynamic 2FL-P400 (c) Dynamic 3FL-P400 (d) Static 1FL-P400 (e) Static 2FL-P400 (f) Static 3FL-P400 - Courtesy of Dillon Betts

CONCLUSIONS

Three specimens were tested under impact with a drop weight at increasing drop heights until failure. The impact resistance and stiffness of the panels increased with facing thickness. The stiffness of each specimen remained relatively constant under the increasing impact energies. Facing strains and maximum deflection both increased with impact energy whereas the damping coefficient decreased. After the failure of the compression face, the stiffness and facing strains of specimen 1FL-P400 decreased drastically and damping coefficient and deflection increased. Based on the test results, the following conclusions were drawn:

- specimen 1FL-P400 resisted a maximum impact of 30.6 J before failure;
- specimen 2FL-P400 resisted a maximum impact of 122.6 J before failure;
- specimen 3FL-P400 resisted a maximum impact of 172.7 J before failure;